HHS Public Access

Author manuscript

J Breath Res. Author manuscript; available in PMC 2019 June 08.

Published in final edited form as:

J Breath Res. ; 12(3): 036020. doi:10.1088/1752-7163/aac5a5.

Power efficient, self-cleaning hydrophilic condenser surface for portable exhaled breath condensate (EBC) metabolomic sampling

Konstantin O. Zamuruyev[a], **Alexander J. Schmidt**[a], **Eva Borras**[a], **Mitchell M. McCartney**[a], **Michael Schivo**[c,d], **Nicholas J. Kenyon**[c,d], **Jean-Pierre Delplanque**[a], and **Cristina E. Davis**[a,*]

[a]Department of Mechanical and Aerospace Engineering, One Shields Avenue, University of California, Davis, Davis, California 95616, U.S.A

[b]School of Veterinary Medicine, 1089 Veterinary Medicine Drive, University of California, Davis, Davis, California 95616, U.S.A

[c]Department of Internal Medicine, Division of Pulmonary and Critical Care Medicine, University of California, Davis, Sacramento, CA 95617, USA

[d]Center for Comparative Respiratory Biology and Medicine, University of California, Davis, Davis, CA 95616, USA

Abstract

In this work, we present a hydrophilic self-cleaning condenser surface for collection of biological and environmental aerosol samples. The condenser is installed in a battery-operated, hand-held breath sampling device. The device performance is characterized with collection and analysis of exhaled breath samples from a group of volunteers. The exhaled breath condensate is collected on a sub-cooled condenser surface, transferred into a storage vial, and its chemical content is analyzed with mass spectrometric methods. The engineered surface supports a continuous condensation cycle on it, and this allows collection of liquid samples exceeding the saturation mass/area limit of a plain hydrophilic surface. The condenser surface employs two constituent parameters: a low surface energy barrier to enhance nucleation and condensation efficiency, and a network of surface microstructures to create a self-cleaning mechanism for fluid aggregation into a reservoir. Removal of the liquid condensate from the condenser surface prevents formation of a thick liquid layer, and thus keeps a continuous condensation cycle with a minimum decrease in heat transfer efficiency as condensation occurs on the surface. The self-cleaning condenser surfaces may have a number of applications in collection of biological, chemical, or environmental aerosol samples. Sample phase conversion to liquid can facilitate sample manipulation and chemical analysis of matrices with low concentrations. Here, we demonstrate the use of a self-cleaning microcondenser for collection of exhaled breath condensate with a hand-held portable device. All breath collections with the two devices were performed with the same group of volunteers under UC Davis IRB protocol 63701-3.

Graphical abstract

*Correspondence: cedavis@ucdavis.edu.

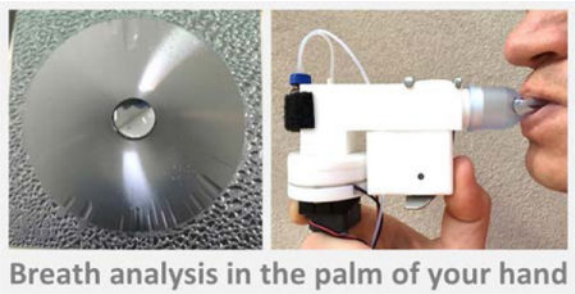

Keywords

exhaled breath condensate (EBC) analysis; portable heath diagnostic; heterogeneous condensation; nucleation energy barrier; heat and mass transfer; hydrophilic self-cleaning condenser surface; capillary micropump

1. Introduction

Energy balance is the fundamental phenomenon that defines the liquid-gas and liquid-solid interface on a surface and drives fluid transport at microscale. Engineered microfluidic devices that take advantage of the Gibbs free energy balance at the solid-liquid-gas interface allow implementation of complex autonomous microsystems that may not require, or significantly minimize, the input of external power and control for their operation. Delicately engineered microscale devices often achieve higher efficiency than their macroscale counterparts. Design of surface energy with chemical treatment and surface micro- or nano-topography finds versatile applications in self-cleaning surfaces [1–5], heat exchangers [6–9], environmental sensors [10], and microfluidic networks for liquid sample delivery, mixing, sorting, or on-chip chemical analysis [10–13]. In this work, we are interested in efficient mass transfer in condensation for the purpose of collecting a biological sample, particularly exhaled breath condensate (EBC) in a miniature hand-held device [14–16].

The theory of droplet nucleation and growth rates in heterogeneous condensation mode was previously described in detail [17–19]. The effect of surface wettability on condensation [8, 9, 20] and heat transfer during droplet nucleation and growth was confirmed with experimental observations [6, 7, 21]. The condensation rate has a strong dependence on surface wettability. Condensation occurs more readily and initially develops at a significantly higher rate on hydrophilic surfaces [6–9, 20]. We employ these concepts to design a small condenser surface with designed microtopography and surface energy to promote initial condensation and support it further by establishing a continuous condensation cycle. The condenser surface is rendered hydrophilic to reduce the nucleation energy barrier and to promote abundant condensation. The liquid film is cleared from the surface with a network of concentric microtopography that employs capillary pressure gradient for fluid transport. The self-cleaning mechanism establishes continuous condensation cycle on the surface by preventing build-up of the liquid film with significant thickness. Otherwise, the condensation would diminish and eventually halt as the

temperature at the liquid-gas interface rises due to the increased thermal resistance across thick liquid layer condensation [6, 7, 21]. Continuous condensation cycle allows collection of sufficiently large amount of liquid sample on a small surface and reduces the power input.

Microfluidic based components are excellent candidates for applications in miniature hand-held systems for personalized health or environment monitoring for recreational or medical purposes. Health diagnostics with metabolomic analysis of exhaled breath can be one of many potential applications. Breath analysis may hold a tremendous promise to advance personalized, noninvasive health diagnostic as new analytical instrumentation platforms and detection methods are developed [22, 23]. EBC contains potentially valuable biomarkers that correlate to other biological fluids such as blood and urine [24, 25] due to gas exchange with blood at the pulmonary alveolar membrane interface [26]. A number of recent case studies demonstrate the feasibility of respiratory, gastrointestinal, and cancer diseases diagnostic with breath analysis due to significant changes in the entire pattern and relative abundances of both, volatile organic compounds (VOCs) and non-volatiles detected in exhaled breath. Breath analysis can be a non-invasive and safe method for health assessment of children with inflammatory diseases such as asthma and cystic fibrosis [27–30], patients with chronic intestinal mycobacteria infection [31], chronic liver disease [32], and oncological diseases [33, 34]. Breath analysis may also find applications in pharmokinetics [35] and exposome monitoring [36].

We envision the use of the self-cleaning condenser surface for collection of EBC in a miniature breath analyzer. The condenser surface is installed in a flow chamber and is cooled with a thermoelectric element installed under it. The vapor in the exhaled breath is condensed on the cooled surface as it passes over it. The saliva filtering module were developed and optimized in our previous work [14]. The conversion to a liquid (denser) phase can facilitate sample manipulation and its chemical analysis when the concentrations are extremely low. In future applications, this self-cleaning condenser surface can also transport the collected EBC sample from the collection unit into an interfaced analytical or storage unit with no external power input required. A set of analytical methods based on mass spectrometric methods are applied to determine the optimal performance of the device for EBC collection. These methodologies can define the significance of the collected EBC metabolic content [37].

2. Material and methods

2.1 Fabrication of the condenser surface

The fabrication of this condenser surface is accomplished with standard microfabrication methods (Figure 1 a). Six inch <100> silicon wafers were cleaned and a layer of 1 μm thick wet thermal oxide was grown in a thermal oxidation furnace. A network of surface topography is defined with lithography in photoresist and then with a wet etch of the thermal oxide layer in 6:1 BOE solution. The surface topography is etched with the DRIE method. The surfaces are diced into individual chips (Disco DAD321) and soaked in a ‘Piranha’ bath (4:1, H_2O_2 (30%):H_2SO_4 (98%)) for 1-2 hours, to clean the surface and render it hydrophilic. The surfaces are thoroughly rinsed with de-ionized (DI) water, dried with N_2, and stored in a clean environment for four days before testing. The etched depth and surface

roughness were verified with a profilometer (Dektak XT®, Bruker Billerica, MA) at three points on the surface. 1 b shows details of the surface topography with images captured with a scanning electron microscope. Supplemental material S1 provides detailed parameters for this fabrication process.

The condenser chip is square (35×35 mm) with a circular micropatterned region (30 mm OD) and a collection reservoir (6 mm OD) at the center. The radial length of concentric microchannels is 12 mm. The micropatterned region is filled with designed geometries enhancing capillary pressure gradient. Two designs, with converging concentric microchannels, are considered in details in this study. One with 943 microchannels separated with straight walls; 10 μm wide at the outer end and 10 μm wide at the inner end, with 6.66 μm/mm radial width gradient in the channels. The other tapered walls; 10 μm wide at the outer end and 14 μm wide at the inner end, with 8.18 μm/mm radial width gradient in the channels.

2.2 Effect of surface energy on droplets nucleation and growth in condensation

Heterogeneous nucleation can be described with classical nucleation theory [17–19]. The free energy barrier, i.e. change in Gibbs energy when a droplet grows, is implicitly defined by the energy of the solid surface in terms of its wettability with the given liquid through their contact angle, the energy of the liquid-vapor interface, and a shape factor of the droplet in terms of its radius and contact angle with the surface.

$$\Delta G = \frac{\pi \sigma_{l\nu} r^{*}(2 - 3\cos\theta + \cos\theta^{3}}{3} \quad \text{Eq. 1}$$

where $\sigma_{l\nu}$ is the surface energy of the liquid-vapor interface, θ is the contact angle of the liquid with the solid surface, and r* is the critical radius of the droplet defined with the Kelvin's equation. The Kelvin equation describes the change in the vapor pressure due to a surface curvature at the liquid-vapor interface.

$$\ln\left(\frac{p_{\nu}}{P_{sat} T_{\nu}}\right) = \frac{2\sigma_{l\nu}}{n_{l} k T_{\nu} r^{*}} \quad \text{Eq. 2}$$

where P_{ν} is the vapor pressure at the temperature close to the condenser surface, P_{sat} is the vapor saturation pressure at the temperature far from the cooled condenser surface, n_l number of molecules per unit volume of liquid, k is the Boltzmann constant, and T_{ν} is the temperature of the condenser surface. The concept of initial embryo formation can be explained with the number of available molecules for its formation. But for the practical purpose of this work, we consider initial droplet formation with the radius above the critical nucleus radius and with the size of the droplet sufficiently large for applicability of Kelvin and Laplace relations [38]. Also, this condenser surface is designed to work in a portable system exposed to exhaled saturated mixture of vapors and gasses ("breath") which is also open to ambient air. This would make exact evaluation theoretically intensive because

condensation conditions change rapidly and are affected by multiple not-controlled changes. The size scale mismatch between molecular scale at nucleation step and uncontrolled meso/macro scale environment may strongly alter the theoretical values too. Thus, this engineering solution provides only an estimation of the physical process.

The rate at which the nuclei of critical size are formed, $J(m^{-2}s^{-1})$, is described with the system conditions.

$$J = J_0 \exp\left(\frac{-\Delta G}{kT_\nu}\right) \quad \text{Eq. 3}$$

where J_0 is a kinetic constant. The creation of small liquid nuclei requires an energy increase. As J increases, the probability that a bubble will exceed critical size and grow into a droplet becomes greater and a spontaneous heterogeneous condensation will occur on the surface more readily.

2.3 Engineering a self-cleaning property – self-actuated capillary flow

The self-cleaning property of the condenser is designed with a network of the surface microtopography. Liquid condensate fluid experiences a self-actuated directional flow toward the central reservoir due to capillary pressure imbalance on the inner and the outer edges of the surface [12, 39]. This self-actuated liquid harvesting mechanism into a liquid dome in the central reservoir makes a continuous condensation cycle possible; otherwise, the condensation would diminish as the condenser surface is covered with a thick layer of liquid. Continuous surface cleaning allows a sufficient amount of liquid sample to be collected on a small surface area with a minimum power input. The aggregated liquid condensate is removed from the central reservoir with a vacuum pump until a required sample volume is collected for consequent chemical analysis.

At microscale, the Navier-Stokes equation simplifies to the Stokes creeping flow [40, 41] because viscous forces dominate over the inertial forces and the flow in capillaries is laminar with small Reynolds number.

$$\eta \nabla^2 u = \nabla P \quad \text{Eq. 4}$$

where η is the fluid dynamic viscosity, $\boldsymbol{u}$ is the fluid velocity, and ∇P is the pressure gradient. Equation 4 is time independent, applying no-slip boundary conditions at the walls of the microchannel and assuming one dimensional flow, it can be simplified [12].

$$\bar{Q} = \frac{1}{\eta}\left(\frac{\Delta P}{R_f}\right) \quad \text{Eq. 5}$$

where R_f is the total flow path resistance, $\bar{Q}$ is the average flow rate, and ΔP is the pressure difference. The surface energy has tremendous power and can be used to drive fluids through

microchannels without any applied pressure [40]. The difference in capillary pressure across the liquid interface at each end of the microchannels establishes differential pressure that actuates the fluid flow. The capillary pressure difference at the interface can be approximated with Young-Laplace equation and relations between curvature, channel size, and contact angle [41].

$$P_c = -\gamma\left(\frac{\cos\theta_t + \cos\theta_b}{d}\right) + \frac{\cos\theta_l + \cos\theta_r}{w} \quad \text{Eq. 6}$$

where γ is the surface tension of the liquid, $\theta_{t,b,l,r}$ are the contact angles of the liquid on the top (air), bottom, left, and right walls, the d and w are the depth and width of the microchannel, respectively.

When satisfying the aspect ratio condition that $d < w$, the flow path resistance in a rectangular microchannel can be approximated with a linear term [10, 12]

$$R_F = \left[\frac{1}{12}\left(1 + \frac{5d}{6w}\right)\left(\frac{dwR_H^2}{L}\right)\right]^{-1} \quad \text{Eq. 7}$$

where L is the length of the microchannel and R_H is the hydraulic radius of the microchannel defined as the ratio of twice the cross-section area divided by the perimeter of the microchannel.

In this work, the width of the microchannel at half-length was used as an average width value. A more exact solution requires in detail solution of the Navier-Stokes equation using a Fourier series approach [42].

2.4 Condensation tests – performance characterization

Two sets of experiments were performed to characterize the engineered surface in condensation. Figure 2 shows the details of the first experimental set-up for condensation. The set-up included a thermoelectric plate (Custom Thermoelectric, Part # 07111-5L31-03CL), heat sink (Digikey, Part # 294-1155-ND), and a brushless fan (Digikey, Part # 259-1541-ND). A reusable nebulizer (LC Plus® by PARI, Part #: 022F81) was used to imitate the saturated air conditions (mass flow rate 440 mg/min, droplet median diameter 3.8 μm). The condenser surface was placed in proximity to the nebulizer outlet nozzle but was not contained in any enclosure with the nebulizer. The saturated air flow was positioned tangentially to the condenser surface to reduce the effect of direct droplet deposition. In this experiment, all condensation tests were purposefully done with uncontrolled ambient conditions (~22°C, ~60% RH) to test the robustness and applicability of the condenser for use in portable medical devices. This set-up provided a benefit of direct visual observation and mass measurement. The experiments were captured on video for timescale observation and comparison. The mass transfer in condensation was evaluated as the difference in the mass of the surface before and after the condensation experiment. The mass of the dry

surface before the experiment and the surface with condensate on it, after the experiment, was measured with an analytical balance (Denver Instruments, Part #: PI-225D).

Once the self-actuated condensate collection was observed, the condenser surface was placed in a miniature breath sampling device. Figure 3 shows the details of the hand-held breath sampling device (25 mm × 50 mm × 120 mm). The device has a disposable mouthpiece, a set of inhale and exhale one-way flap valves to allow condensation of exhaled breath only, and a saliva filter. The operation principle of the saliva filter is described in details in our earlier work [14]. The new device is made smaller to ensure portability and future integration with miniature microfluidic analytical modules. It is constructed from materials with different surface properties, and operates at a higher temperature level than in our previously described EBC sampler [14]. The 310 mm long borosilicate glass tube, cooled with dry ice pellets (−56°C), is substituted with a 35×35 mm Si/SiO_2 microcondenser element, cooled with a thermoelectric element. This allows reduction in size and power consumption. The thermoelectric plate (Custom Thermoelectric Part # 07111-5L31-03CL) requires 6.5V and 0.7A to keep the EBC collector surface at 5 ± 2°C. The new cooling method affected the temperature level of the collector surface. Two types of batteries were used in these experiments. One with 2200 mAh capacity, 5V, 1A output (Adafruit, Part # 1959); it lasted 1 hour. A more powerful battery with 10000 mAh capacity, 5V, 2.1A/1A 2-port output (Adafruit, Part #1566) lasted for 2 hours in continuous use.

The second set-up with enclosed surface allowed more practical measurements of condensation rate. The condensation rate was measured with two fluids: deionized water and saline solution (SIGMA #P3813-10PAK). The nebulizer flow, imitating exhaled breath, was directed into the inlet of the breath sampling device; first with deionized water and then with a saline solution.

To demonstrate a continuous condensation cycle and its benefit to collect virtually unlimited amount of sample on a small surface, the condensate liquid dome was periodically extracted from the central reservoir with a vacuum pump (AIRPO™ Part #: D2028B) into a 2 mL vial (Agilent #5190-2280) that was placed on an analytical balance (Denver Instruments, Part #: PI-225D). The tip of the capillary tube (fused-silica, 360μm OD, 250μm ID, 37 mm long; LabSmith, Part #: CAP360-250S) was placed into the central collection reservoir of the microcondenser and inserted into the vial, as shown in Figure 3b. The vacuum pump was controlled with an Arduino Uno microcontroller at the duty cycle of 10 seconds, reoccurring every 30 seconds. Pinnacle USB 1.2 software was used to collect real time mass measurement data at 2 second intervals from the analytical balance. The data for the condensate sampling rate using this set-up with the enclosure is provided in Figure 5.

2.5 Exhaled breath condensate collection and analysis

To demonstrate the performance of this mini EBC-sampler, EBC samples were collected from a group of six healthy volunteers representing three age groups of 20, 30, and 40 years old and two gender groups (3 males and 3 females). All participants were in good health, with no history of smoking. To reduce confounding factors, volunteers restrained from consuming food for 2 h before sampling, and rinsed their mouths with drinking water before sampling. A clean collection device was assembled and allowed to cool for 5 min before

sampling. Each participant sat in a relaxed, upright position during the collection. All participants were asked to breathe normally (tidal breathing) into the device for a 40 minute period. This elongated sampling time was to ensure we had sufficient amount of EBC sample to perform mass spectrometry analysis with different methods. During sampling, the EBC sample was transferred from the central collection reservoir on the condenser surface into a clean borosilicate vial, cap sealed, weighed, and placed into a −80°C freezer for storage. This process was repeated until >1 mL of EBC was collected from each participant. All parts of the collection device were thoroughly cleaned before and after each use. The cleaning protocol included three rinses: deionized (DI) water rinse, followed by 70% ethanol disinfectant rinse, followed by DI water rinse and drying.

In order to benchmark the performance of this mini EBC-sampler, it was compared to a larger scale version of an EBC sampler that had previously been characterized in comparison to two commercial devices [14]. The effect of differences in EBC collection temperature and surface material were considered. EBC samples were collected at 5°C and −56°C with the previously described instrument (glass tube). All EBC collections with the two devices were performed with the same group of volunteers under UC Davis IRB protocol 63701-3.

Three groups of individual EBC samples were collected from the six volunteers; one with the mini-EBC sampler operating at 5°C, the other two with the previously characterized instrument (glass tube) operating at 5°C and −56°C. These three groups of samples allowed to consider effects of the collection temperature and surface materials on metabolomic content of EBC. In order to reduce the effect of physiological differences among volunteers, three “averaged” 6 mL EBC samples were prepared. One mL aliquots from each participant were pooled to create an “averaged” EBC sample, per each device and each temperature.

The metabolomic content of EBC sample was obtained by applying a set of analytical methods to cover a wide spectrum of compounds. Each “averaged” EBC sample was aliquoted into separate vials containing 1 mL for GC-MS analysis, two vials with 0.5 mL for LC-MS RP analysis, and two vials with 0.5 mL for LC-MS HILIC analysis. The vials were capped with PTFE/silicone septa and stored at −80°C until further analyses.

The volatile fraction was analyzed with gas chromatography-mass spectrometry (GC-MS) methodology as previously described [14, 37]. The vial-sealed EBC aliquots were allowed to thaw and volatile fraction was extracted using a polyacrylate (PA) solid-phase microextraction (SPME) (Supelco, Bellefonte, PA) tip during 30 min period with samples kept at room temperature. Samples were analyzed with a Varian 3800 GC (Varian, Walnut Creek, CA) and a 4000 Ion Trap MS (Varian) equipped with electron ionization source (EI) instrument. To assure the accurate analysis, DI water and empty vial blanks and quality controls of aqueous D8 naphthalene solution was also analyzed.

The non-volatile fraction was analyzed with optimized liquid chromatography-mass spectrometry (LC-MS) methods based on previous studies [14, 37]. For LC-MS, we applied two complimentary methods to cover a wide range of non-volatile compounds. The non-polar and lipid metabolites were covered with a reverse-phase (RP) and more polar compounds with a hydrophilic interaction LC (HILIC).

For LC-MS analysis, EBC samples were pre-concentrated by a prior lyophilization. The freeze-dried extract was re-dissolved in 60 μL of HPLC grade acetonitrile:water 1:1 v/v. 15 μL were injected twice per sample in an Agilent 1290 binary high-performance liquid chromatography (HPLC) system coupled to an Agilent 6530 Q-TOF mass spectrometer (Agilent Technologies, Santa Clara, CA) using an AJS electrospray ionization system working in positive mode at a mass range from 50 to 1200 m/z. For the RP analysis, an Infinity Poroshell 120 EC-C18 column (3 × 50 mm, 2.7 μm; Agilent Technologies, Palo Alto, CA) was used at 30°C. Mobile phase gradient consisted of water (A) and acetonitrile (B), both at 0.1% of formic acid.

For the HILIC analysis, a Waters Acquity UPLC BEH Amide 130 Å (2.1 × 100 mm, 1.7 μm; Waters, Milford, MA) column was used at 40°C. In this case, a gradient of mobile phase was applied using an ammonium formate aqueous solution at 50 mM (adjusted at pH 3.2 with formic acid) mixed with acetonitrile:50mM NH4 formate 90:10 (v/v) (A) and acetonitrile:water:50mM NH4 formate 50:40:10 (v/v) (B). Solvent blanks and quality controls were also run in each method, using Waters 6963 RP QC and Waters 186006963 HILIC QC (Waters, Milford, MA) for RP and HILIC, respectively.

Collected MS data was first visualized using MS Data Review software v. 6.6 (Varian) for GC-MS and Agilent's Mass Hunter Qualitative Analysis B.06.00 software for LC-MS. GC-MS peaks were first deconvolved using Automated Mass Spectral Deconvolution and Identification System (AMDIS) software v. 2.64, following by a peak alignment between samples using Mass Profiler Professional 13.1 software. LC-MS peaks were deconvolved and aligned simultaneously using Agilent's Mass Hunter Profinder B.08.00 software and "Batch Recursive Feature Extraction" algorithm.

3. Results and discussion

3.1 Condensation cycle and its implication for heat transfer

In this application of the condenser surface for collection of a biological sample, we are interested more in the efficient mass collection rather than heat transfer – but the two processes are primarily related. The amount of heat transferred in a latent process, e.g. a phase change from vapor to liquid, may far exceed the amount of heat transferred in conduction and convection processes. Thus, a well-designed collector for rapid condensation of vapor samples is also an excellent heat exchanger. To increase the amount of mass transfer, we made the surface hydrophilic to promote condensation on it. To avoid surface saturation, we engineered a surface microtopography that actuates fluid aggregation, and thus prevents accumulation of a thick layer of condensate on it. This surface property, in conjunction with a mechanical fluid removal from the collection reservoir, establishes a continuous condensation cycle that allows virtually unlimited amount of liquid sample to be collected on a small surface area with minimum power input.

Figure 4 shows the microcondenser surface in condensation. The surface is placed on a thermoelectric cooler and is open to ambient air. A supplemental video SV1 demonstrates fluid aggregation in the form of a dome in the central reservoir. For this open-to-air set-up, the duty cycle of the vacuum pump was changed. The condensation accumulation period

was lengthened to 55 seconds and the condensate removal period shortened to 5 seconds because most of the vaporized flow from the nebulizer disseminated in atmosphere before making contract with the surface.

Figure 4a shows the surface at four minutes after its exposure to the imitated vapor flow. The surface is hydrophilic, strong patch-like condensation occurs on the edges of the condenser where the surface is flat. Patch-like droplet growth is prevented on the circular micropatterned region. The bulk of condensate liquid is self-aggregated into the central collection point. Only microchannel cavities are filled and covered with a thin film of liquid. Once the droplet at the central reservoir gets filled into a full hemisphere, the droplet pressure equilibrates with the capillary pressure in the microchannels and the capillary flow stops. Further condensation without removal of the fluid from the central reservoir, will lead first to overflow in the microchannels on their outer ends, seen as wave streaks in the photo, and then to rupture of the central droplet onto the micropatterned surface. If condensation is continued, the surface will become fully covered with a thick layer of condensate liquid. The condensation rate will diminish and eventually stop due to thermal resistance of the thick liquid layer covering the surface. At that point, additional mass accumulation will likely to be mainly due to direct deposition of fine respiratory droplets carried from the breath to the surface of the liquid. A continuous condensation cycle avoids surface saturation and allows operation near the efficiency peak; both condensation and direct droplet deposition contribute to the mass accumulation.

These qualitative experimental observations agree with the works of other researches [6, 7, 9, 20, 21] that describe heterogeneous nucleation and condensation. We did not quantify the mass transfer decrease rate since the goal of this work was to design a device with small size and power input for efficient collection of biological samples, particularly a portable breath sampler.

Figure 4b demonstrates a continuous condensation cycle on the surface. Microtopography of the surface aggregates condensate from the surface into a liquid dome at the collection point. The liquid dome is periodically removed with a capillary tube connected to a vacuum pump. The retrieved condensate liquid is accumulated in a vial. The self-actuated collection of fluid into a reservoir is repeatable and allows collection of condensate volumes that highly exceed the area size of the surface. Figure 4b shows one cycle: the condensate is self-aggregated at the collection point (6:30), this volume of condensate fluid is retrieved with a vacuum pump (6:45), a new self-aggregated volume of condensate fluid is formed at the collection point (7:15), and retrieved with a vacuum pump (7:20). A supplemental video SV2 demonstrates the continuous condensation cycle.

Hydrophilic surfaces are prone to ambient contamination as they attract water molecules and water soluble compounds [43]. To maintain the property of the surface, the condenser surfaces had to be re-cleaned with 4:1 Piranha solution and rinsed with DI after each EBC sampling because the surface performance degraded due to ionic contamination. The cleaned surfaces were stored in a clean hermetic enclosure for a sufficient period of time to reduce the superhydrophilic state of the surface after Piranha cleaning. The surfaces were used for experiments and EBC collection 4 days after cleaning. The strong hydrophilicity of the

surface degrades and the water contact angle increases to ~35° which seems to be a sufficient level for fluid aggregation to occur [43, 44]. Supplemental material S2 shows the dependence of the energy barrier and nucleation rate on surface wettability and temperature difference between the condenser surface and the vapor flow. The surface wettability is a significant factor defining the rate of condensation and therefore effectiveness of heat and mass transfer. Comparison of a hydrophilic surface with a contact angle of 30° to a hydrophobic surface with a contact angle of 110°, yields an increase in energy barrier of about 60 times resulting in decrease in the nucleation rate by a factor of $3 * 10^{101}$. The temperature difference between the cold surface and the ambient vapor has a weaker effect on the energy barrier and nucleation rate than the surface wettability. Thus, a designed surface wettability may result in a higher condensation efficiency and a reduced power input for cooling of a condenser surface. This is highly desirable for hand-held portable applications.

In this design, a network of concentric microchannels is used for aggregation of liquid condensate from the surface. The liquid propagates in the channels due to capillary pressure misbalance. The capillary pressure is more negative at the narrow end than at the wider end. Supplemental video SV3 demonstrates the directional fluid flow toward the central reservoir. DI water is introduced from the outer edge of the patterned region; surface and water are at 25°C. The fluid is transported into the radial direction, enters the central reservoir, and accumulates at its inner edge. The pressure difference in the microchannels can be enhanced by increasing the difference in width between the outer and the inner end of the microchannels. Two designs with concentric microchannels were tested. The design difference was reflected in experimental tests with very small practical difference in condensate accumulation rates. It is likely that the improvement of the second design with the tapered walls and increased radial width gradient was counterbalanced by the greater number of microchannels in the first design. Due to small difference in condensation rate, no further characterization was made. To characterize the effect of radial width gradient on the flow rates in the capillaries two surfaces with equal number of channels would be required.

Surface topography may serve not only as a passive, geometry-based, capillary pump for the self-actuated fluid flow towards the collection reservoir but it also may contribute to the heat transfer efficiency of the condenser. Microtopography can significantly increase the available surface area for condensation due to additional area of its vertical planes. In this case, eight hundred concentric microchannels etched to the depth of 60 μm provide an additional 170% to the top plain condenser surface area for condensation. Another important contribution of the surface topography to the heat transfer is that the bottom corner edge and narrow spaced geometries provide nucleation sites for capillary condensation. The unique aspect of capillary condensation is that vapor condensation occurs below the saturation vapor pressure on concave surface as described by the Kelvin and Young-Laplace equations. Thus, at a concave interface, condensation can occur at slightly higher temperature in ambient conditions which reduces a power input to cooling element and enhances the heat transfer in condensation. A surface with eight 800 concentric microchannels makes an effective length of 19.2 m of corner line. These nucleation sites in the corner line, where condensation occurs early and quickly, can be a significant contribution to the heat exchange. Supplemental material S3 provides more details on engineering surface

microtopography; dependence of surface area and capillary pressure gradient on the number of channels, dependence of capillary flow on surface wettability and channel depth and width gradient.

3.2 EBC sampling rate estimation

The first experimental set-up, as shown in Figure 2, provided only visual confirmation of the fluid self-aggregation and a continuous condensation cycle. To estimate the sampling rate, the surface was enclosed in the mini EBC sampler housing as shown in Figure 3. The aerodynamic mass filter is designed to extract aerosol droplets with diameter of 100 μm or larger from the flow, route the flow over the condenser surface, and prevent condensation from the ambient air [14].

Figure 5a shows a calibration curve for sampling rate with a controlled flow. A vaporized flow from a nebulizer was connected to the inlet (mouthpiece) of the mini EBC sampler. The condensate was transferred from the condenser surface into a vial with a capillary tube connected to a vacuum pump. The retrieved condensate mass in a vial was measured with an analytical balance. Two condenser designs with different number of microchannels and two sample fluids, such as DI water and saline solution were tested with the controlled flow. Condensation of saline solution was used to imitate condensation of EBC where change in viscosity or presence of salts may affect the condensation rate. Condensation tests were repeated three times for each condenser design and type of fluid. An average of three runs is plotted in Figure 5a. The error bars for three test runs are not shown due to negligible deviation from the average value. The three runs were performed with different condenser surfaces to confirm that device to device variability is acceptable.

Figure 5b shows sampling rates of EBC from six volunteers. The data points are based on a single measurement from each volunteer. In this case, the flow is not controlled and reveals the physiological and breathing rate differences. The EBC sampling rate depends on multiple factors, the main of which is the total volume of exhaled breath [45, 46]. Based on our previous experience with EBC sampling using commercial and engineered devices [14], the wide variation among volunteers can be normal. The main purpose of this controlled experiment was not to imitate the condensation process but to test consistent performance of the condenser surface over a prolonged period of time (40 min) with a controlled flow, and then see that the sampling rate differences in EBC were mostly due to physiological and breathing differences among volunteers rather than the surface performance. The overall increase between the condensation rate shown in Figure 5a and 5b is expected due to a number of differences in the flow conditions; the total volumetric flow rate (L/min) between the nebulizer device and the humans, the temperature (25°C versus 36°C) and humidity of the flow passing over the condenser surface. EBC sampling can be standardize with the use of a feedback regulated sampling device [46].

Though, the total condensate mass is small, the sampling rate of this mini EBC sampler is twice as high compared to commercial EBC samplers, if compared per surface area of the condenser element. Based on our previous study [14], the EBC sampling rate is 0.68 $mg/cm^2/min$ for RTube™ (Respiratory Research, Inc., Austin, TX, USA; condenser surface area 157 cm^2, Avg. mass 1.08 g/10 min) and 1.40 $mg/cm^2/min$ for TurboDECCS

(MEDIVAC, Parma, Italy; condenser surface area 91.30 cm^2, Avg. mass 1.28 g/10 min). The sampling rate of this hand-held microcondenser based EBC sampler is 2.82 mg/cm^2/min (surface area 7.07 cm^2, Avg. mass 0.20 g/10 min). Also note that the net mass of EBC collected with each device may not fully represent the condensation efficiency per surface area of the condenser element because some volume of sample is lost during sample retrieval from the device into a storage container. Here, the EBC data is the net mass of the retrieved sample.

We note that EBC sampling over 40 minutes time period is unnecessary long and not practical for a portable self-diagnostic platform. It was necessitated due to size scale mismatch between the microscale condenser element and the bench top instruments used for chemical characterization of the collected EBC sample. The minimum sample volume for bench top mass spectrometers highly exceeds the limits of microfluidics. The amount of sample collected could be reduced to a few microliters and the sampling time reduced to 2-3 minutes when both collection and analysis are possible to be done in a microscale system [47].

3.3 Breath metabolomics with mini-EBC sampler

The metabolomic content of EBC is known to be affected by a number of factors [48, 49]. The hardware factors may include: adhesive and chemical properties of the collector surfaces that are in contact with exhaled breath, saliva contamination of the collected sample, and condensation temperature. To confirm the legitimacy of the hand-held EBC sampler to collect metabolomic informative EBC samples, we collected EBC samples from a group of six healthy volunteers.

The mini-EBC sampler collects between 100 and 400 μL of EBC depending on the variation among subjects (Figure 5b) and other factors [45]. We considered the effect of sample volume variation on our ability to detect metabolomic compounds. We intended to determine the minimum amount of EBC that will diminish the chromatographic response. For this, we collected, equally aliquoted, and pooled EBC samples from four healthy volunteers. The pooled samples were aliquoted at different volumes prior the lyophilization and analysis. LC-MS samples require a lyophilization step to remove water and allow working with an organic solvent required for the LC-MS method. Otherwise, there is variability due to different solvents present in the samples; these may alter the signal responses due to the matrix itself and not the samples [50]. The analysis was performed as previously described. The described methodology [14, 37] has a factor of concentration of 8.3, using 0.5 mL of EBC to freeze-dry and reconstitute after in 60 μL of mobile phase. Here, we tested concentration factors between 1 and 8.3. Figure 6 shows the effect of the non-volatile metabolites concentrated from EBC. Chromatographic profiles show a diminishment in the acquired signal when concentration factors are lowered for both, RP and HILIC (Figure 6 a). When the number of peaks are counted, after the data treatment, we observe that at concentration factors lower than 3.3 (200 μL of EBC dried and reconstituted in 60 μL) less than 75% of the metabolites found at the highest concentration can be detected (Figure 6 b). It’s important to notice that some of the metabolites with the higher relevance (potential biomarkers) for biological and environmental studies are present at low levels of

concentration. For this, we conclude that the minimum EBC sample volume is 200 μL for mass spectrometry analysis.

In order to benchmark the performance of this mini EBC-sampler, it was compared to a larger macro-scale EBC sampler that had earlier been characterized in comparison to two commercial devices: RTube™ and TurboDECCS [14]. The two main differences between the mini EBC sampler and the macro EBC sampler are that they use different condenser elements, Si/SiO_2 instead of glass tube, and operate at different temperatures, +5°C instead of −56°C. To check these two design differences, additional EBC samples were collected from the same group of six volunteers with the EBC sampler that had a glass tube. To check the effect of surface material, additional EBC samples were collected with the glass condenser surface maintained at the same temperature as that of the microcondenser (+5°C). To check the effect of temperature difference, additional EBC samples were collected from the same six volunteers with the glass tube condenser kept at −56°C.

The six individual samples, collected with each experimental condition, (total 18 samples) were equally aliquoted and pooled to represent an average EBC sample from a healthy person per each sampling set-up. Each group of samples had three technical replicates. The three groups of the EBC samples were analyzed with a GC-MS method to detect volatile fraction and two different LC-MS methods for the non-volatile fraction.

Figure 7 compares the chromatographic profiles obtained with GC-MS (Figure 7a), LC-MS HILIC (Fig. 7b) and LC-MS RP (Fig. 7c) methodologies for the mini-EBC sampler and the previously described EBC sampler operated at +5°C and −56°C. For each group, the three replicates show excellent repeatability. Both GC-MS and LC-MS analyses do not show significant differences between the EBC samples collected with Si/SiO_2 microcondenser and glass condenser tube. The difference in temperature level of the condenser element seems to have a weak effect on the chromatographic profile too. Thus, we may conclude that the performance of the battery operated mini-EBC sampler is adequate. The small size and low power consumption may make it an excellent candidate for integration with miniature analytical systems for portable analysis.

To quantify these differences, the number of detected peaks was calculated for each experimental set-up. Table 1 summarizes the number of the representative metabolites for each experimental set-up and analytical method. The raw data was first deconvoluted and aligned as previously described. A detected peak was considered present if it satisfied three criteria. The peak abundance was above 5000 a.u. for GC-MS and 3000 a.u. for LC-MS. The peak was observed in, at least, two out of three technical replicates. The peak was not present in blanks. For a peak that was present in both, sample and blanks, the abundance a ratio of sample/blank was used. Any peak with the ratio of sample/blank abundance lower than 10 was discarded. There was a small difference in the number of detected compounds that may resemble differences in operating temperature or surface materials of the two devices.

For the volatile compounds detected with GC-MS, more peaks were detected in EBC samples collected with the glass tube device when it was operated at a at −56°C in

comparison to EBC samples collected with the same device operated at +5°C. The number of volatile compounds was equal when comparing the mini EBC sampler with the glass tube device when both were operated at +5°C. This observation is in agreement with our recent study on the effect of collection temperature on the metabolomic content of EBC samples [51].

For the non-volatile compounds detected with LC-MS, more compounds were detected in EBC samples collected with the glass tube device operated at −56°C (750 metabolites) with LC-MS RP and with the same device operated at +5°C (600 metabolites) with LC-MS HILIC. The number of detected non-volatile compounds was lower by 15 % in the EBC samples collected with the mini-EBC sampler for both methods: LC-MS RP and LC-MS HILIC. Since the number of detected compounds was lower for both methods, it can be due to the surface property effects rather than the temperature difference.

4. Conclusions

This work presents the design of a microcondenser surface for applications in personal health diagnostic with breath analysis. The microcondenser demonstrates a self-actuated method to aggregate the condensate sample into a common reservoir. The engineered misbalance of capillary pressure drives the fluid in the predetermined direction. The fabricated surfaces demonstrated robust performance in multiple uses and after being stored and re-cleaned after each use. This capillary pressure pump is applicable to a variety of fluids, though the dimensions of the microtopography may need to be adjusted for the properties of a particular fluid. The observed experimental results during condensation are in high accordance with the previously described theory and experimental trials. The surface establishes a continuous condensation cycle that prevents formation of a thick layer of condensate liquid and allows collection of virtually unlimited amount of condensate on a small area surface. The microcondenser could also potentially operate as a passive condensate collector in an environmental chamber/pollutant/air quality sampler.

Here we considered and quantified its application for collection of a biological sample. The surface was installed into a portable, battery-operated, EBC sampler. The device applicability to collect chemically informative breath samples was confirmed with comparison of its performance to an earlier quantified EBC collector and with extensive chemical analysis of the collected EBC samples. One of the main breakthroughs of this work is that a delicately engineered surface with a microscale mechanism could surpass the challenges of the size-scale mismatch between the micro actuating mechanism and macro world ambient environment. It surpassed one of the main limitations of the microfluidic devices – to operate in an uncontrolled environment where the scale of disturbances such as contamination sources may far exceed the microscale engineered mechanisms. The invention of self-actuated directional fluid transport may make a significant contribution to future designs of totally integrated microsystems on a chip or wafer scale where sample collection and analysis are done with a microscale quantities and minimum power and control input.

Software and device design information

The software code and PCB design specifications for our portable exhaled breath condensate (EBC) metabolomic sampling device are available on GitHub. Please refer to Professor Cristina Davis' webpage for more information. This material is available as open source for research and personal use under a modified BSD license. Commercial licensing may be available, and a license fee may be required. The Regents of the University of California own the copyrights to the software and PCB designs. Future published scientific manuscripts or reports using this software and/or hardware designs must cite this original publication (DOI: xxxxxxxxxxxx).

Supplementary Material

Refer to Web version on PubMed Central for supplementary material.

Acknowledgments

Partial support was provided by: NIH award U01 EB0220003-01 (CED, NJK); the NIH National Center for Advancing Translational Sciences (NCATS) through grant UL1 TR000002 (CED, NJK); NIH award 1P30ES023513-01A1 (CED, NJK); and The Hartwell Foundation (CED, NJK), Student support was provided by NIH award T32 HL07013 (KOZ), and NIH award P42ES004699 (KOZ). The contents of this manuscript are solely the responsibility of the authors and do not necessarily represent the official views of the funding agencies. The authors gratefully acknowledge access and use of the Marvel Nano Laboratory recharge facility (University of California, Berkeley).

Appendix A. Supplementary data

Supplementary data related to this article can be found at **xxx**.

References

1. Sahoo BN, Kandasubramanian B. Recent progress in fabrication and characterisation of hierarchical biomimetic superhydrophobic structures. Rsc Advances. 2014; 4(42):22053–22093.
2. Zamuruyev KO, et al. Continuous Droplet Removal upon Dropwise Condensation of Humid Air on a Hydrophobic Micropatterned Surface. Langmuir. 2014; 30(33):10133–10142. [PubMed: 25073014]
3. Bhushan B, Jung YC, Koch K. Self-Cleaning Efficiency of Artificial Superhydrophobic Surfaces. Langmuir. 2009; 25(5):3240–3248. [PubMed: 19239196]
4. Yao ZW, Bowick MJ. Self-propulsion of droplets by spatially-varying surface topography. Soft Matter. 2012; 8(4):1142–1145.
5. Feng J, et al. Why Condensate Drops Can Spontaneously Move Away on Some Superhydrophobic Surfaces but Not on Others. Acs Applied Materials & Interfaces. 2012; 4(12):6618–6625. [PubMed: 23153202]
6. Miljkovic N, Enright R, Wang EN. Effect of Droplet Morphology on Growth Dynamics and Heat Transfer during Condensation on Superhydrophobic Nanostructured Surfaces. Acs Nano. 2012; 6(2):1776–1785. [PubMed: 22293016]
7. Rykaczewski K. Microdroplet Growth Mechanism during Water Condensation on Superhydrophobic Surfaces. Langmuir. 2012; 28(20):7720–7729. [PubMed: 22548441]
8. Varanasi KK, et al. Spatial control in the heterogeneous nucleation of water. Applied Physics Letters. 2009; 95(9)
9. Zhao H, Beysens D. From Droplet Growth to Film Growth on a Heterogeneous Surface - Condensation Associated with a Wettability Gradient. Langmuir. 1995; 11(2):627–634.

10. Delamarche E, et al. Microfluidic networks for chemical patterning of substrate: Design and application to bioassays. Journal of the American Chemical Society. 1998; 120(3):500–508.
11. Leu TS, Chang PY. Pressure barrier of capillary stop valves in micro sample separators. Sensors and Actuators a-Physical. 2004; 115(2–3):508–515.
12. Zimmermann M, et al. Capillary pumps for autonomous capillary systems. Lab on a Chip. 2007; 7(1):119–125. [PubMed: 17180214]
13. Gillmor SD, et al. Hydrophilic/hydrophobic patterned surfaces as templates for DNA arrays. Langmuir. 2000; 16(18):7223–7228.
14. Zamuruyev KO, et al. Human breath metabolomics using an optimized non-invasive exhaled breath condensate sampler. Journal of Breath Research. 2017; 11(1)
15. Zamuruyev KO, et al. Enhanced non-invasive respiratory sampling from bottlenose dolphins for breath metabolomics measurements. Journal of Breath Research. 2016; 10(4)
16. Aksenov AA, et al. Metabolite Content Profiling of Bottlenose Dolphin Exhaled Breath. Analytical Chemistry. 2014; 86(21):10616–10624. [PubMed: 25254551]
17. Carey, VP. Series in chemical and mechanical engineering. Washington, D.C.: Hemisphere Pub. Corp.; 1992. Liquid-vapor phase-change phenomena: an introduction to the thermophysics of vaporization and condensation processes in heat transfer equipment; p. 169-206.p. 337-389.
18. Friedlander, SK. Topics in chemical engineering. 2nd. New York: Oxford University Press; 2000. Smoke, dust, and haze: fundamentals of aerosol dynamics; p. xx, 407
19. Porter, DA., Easterling, KE., Sherif, MY. Phase transformations in metals and alloys. 3rd. Boca Raton, FL: CRC Press; 2009. p. xix, 500
20. Pulipaka S, Son SY. Study of effect of wettability on heterogeneous condensation-varied substrates. Proceedings of the Asme International Mechanical Engineering Congress and Exposition 2007. 2008; 8:1125–1130. Pts a and B.
21. Enright R, et al. Condensation on Superhydrophobic Surfaces: The Role of Local Energy Barriers and Structure Length Scale. Langmuir. 2012; 28(40):14424–14432. [PubMed: 22931378]
22. Amann A, Smith D. Volatile Biomarkers Non-Invasive Diagnosis in Physiology and Medicine Foreword. Volatile Biomarkers: Non-Invasive Diagnosis in Physiology and Medicine. 2013:Xxvii–Xxix.
23. Buljubasic F, Buchbauer G. The scent of human diseases: a review on specific volatile organic compounds as diagnostic biomarkers. Flavour and Fragrance Journal. 2015; 30(1):5–25.
24. Amann A, et al. The human volatilome: volatile organic compounds (VOCs) in exhaled breath, skin emanations, urine, feces and saliva. Journal of Breath Research. 2014; 8(3)
25. Stiegel MA, et al. Analysis of inflammatory cytokines in human blood, breath condensate, and urine using a multiplex immunoassay platform (vol 20, pg 35, 2014). Biomarkers. 2015; 20(1):E97–E97. [PubMed: 25613492]
26. Phillips M. Breath Tests in Medicine. Scientific American. 1992; 267(1):74–79. [PubMed: 1502511]
27. Baraldi E, et al. Safety and success of exhaled breath condensate collection in asthma. Archives of Disease in Childhood. 2003; 88(4):358–360. [PubMed: 12651772]
28. Markar SR, et al. Exhaled Breath Analysis for the Diagnosis and Assessment of Endoluminal Gastrointestinal Diseases. Journal of Clinical Gastroenterology. 2015; 49(1):1–8. [PubMed: 25319742]
29. Kramer R, et al. A rapid method for breath analysis in cystic fibrosis patients. European Journal of Clinical Microbiology & Infectious Diseases. 2015; 34(4):745–751. [PubMed: 25431363]
30. Shestivska V, et al. Quantitative analysis of volatile metabolites released in vitro by bacteria of the genus Stenotrophomonas for identification of breath biomarkers of respiratory infection in cystic fibrosis. Journal of Breath Research. 2015; 9(2)
31. Purkhart R, et al. Chronic intestinal Mycobacteria infection: discrimination via VOC analysis in exhaled breath and headspace of feces using differential ion mobility spectrometry. Journal of Breath Research. 2011; 5(2)
32. Eng K, et al. Analysis of breath volatile organic compounds in children with chronic liver disease compared to healthy controls. Journal of Breath Research. 2015; 9(2)

33. Kumar S, et al. Mass Spectrometric Analysis of Exhaled Breath for the Identification of Volatile Organic Compound Biomarkers in Esophageal and Gastric Adenocarcinoma. Annals of Surgery. 2015; 262(6):981–990. [PubMed: 25575255]
34. Capuano R, et al. The lung cancer breath signature: a comparative analysis of exhaled breath and air sampled from inside the lungs. Scientific Reports. 2015; 5
35. Beauchamp J. Inhaled today, not gone tomorrow: pharmacokinetics and environmental exposure of volatiles in exhaled breath. J Breath Res. 2011; 5(3):037103. [PubMed: 21654021]
36. Spanel P, Dryahina K, Smith D. A quantitative study of the influence of inhaled compounds on their concentrations in exhaled breath. Journal of Breath Research. 2013; 7(1)
37. Aksenov AA, et al. Analytical methodologies for broad metabolite coverage of exhaled breath condensate. J Chromatogr B Analyt Technol Biomed Life Sci. 2017; 1061–1062:17–25.
38. Thompson SM, et al. A Molecular-Dynamics Study of Liquid-Drops. Journal of Chemical Physics. 1984; 81(1):530–542.
39. Berthier J, Brakke KA, Berthier E. A general condition for spontaneous capillary flow in uniform cross-section microchannels. Microfluidics and Nanofluidics. 2014; 16(4):779–785.
40. Brody JP, et al. Biotechnology at low Reynolds numbers. Biophysical Journal. 1996; 71(6):3430–3441. [PubMed: 8968612]
41. Ichikawa N, Hosokawa K, Maeda R. Interface motion of capillary-driven flow in rectangular microchannel. Journal of Colloid and Interface Science. 2004; 280(1):155–164. [PubMed: 15476786]
42. Spurk, J., Aksel, N. Fluid Mechanics. Springer Berlin Heidelberg; 2008.
43. Drelich J, et al. Hydrophilic and superhydrophilic surfaces and materials. Soft Matter. 2011; 7(21): 9804–9828.
44. Takeda S, et al. Surface OH group governing adsorption properties of metal oxide films. Thin Solid Films. 1999; 339(1–2):220–224.
45. Gessner C, et al. Factors influencing breath condensate volume. Pneumologie. 2001; 55(9):414–9. [PubMed: 11536064]
46. Winters BR, et al. Standardization of the collection of exhaled breath condensate and exhaled breath aerosol using a feedback regulated sampling device. J Breath Res. 2017; 11(4):047107. [PubMed: 28894051]
47. Willis PA, Creamer JS, Mora MF. Implementation of microchip electrophoresis instrumentation for future spaceflight missions. Analytical and Bioanalytical Chemistry. 2015; 407(23):6939–6963. [PubMed: 26253225]
48. Horvath I, et al. Exhaled breath condensate: methodological recommendations and unresolved questions. European Respiratory Journal. 2005; 26(3):523–548. [PubMed: 16135737]
49. Rosias PP, et al. Breath condenser coatings affect measurement of biomarkers in exhaled breath condensate. European Respiratory Journal. 2006; 28(5):1036–1041. [PubMed: 16870660]
50. Fernandez-Peralbo MA, et al. Study of exhaled breath condensate sample preparation for metabolomics analysis by LC-MS/MS in high resolution mode. Talanta. 2015; 144:1360–9. [PubMed: 26452970]
51. O ZK, et al. Effect of temperature control on the metabolite content in exhaled breath condensate. Analytica Chimica Acta. 2018; 1006:49–60.

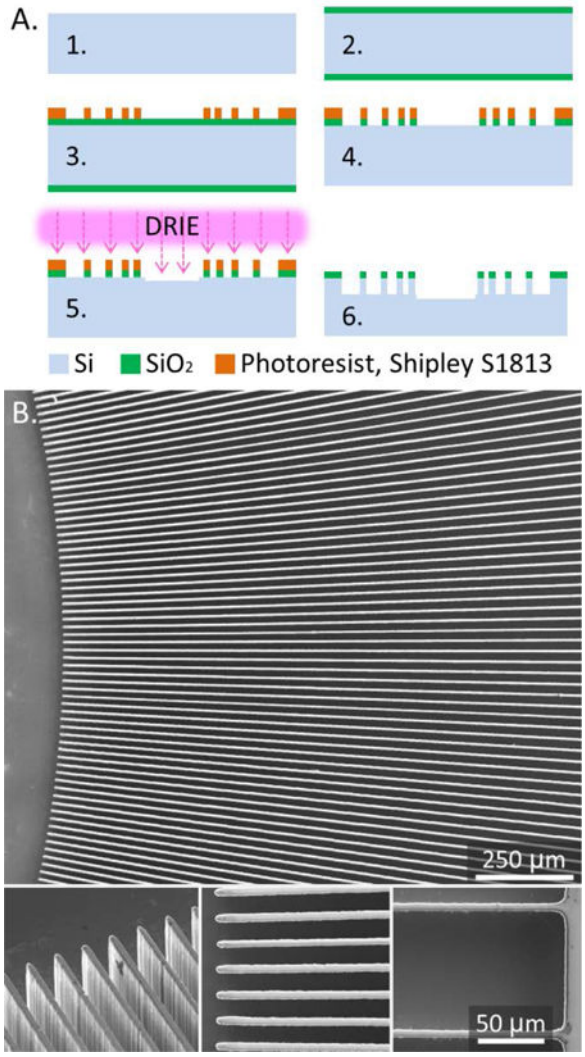

Figure 1.

A. Microfabrication process: 1. Clean the wafer, 2. Grow a layer of thermal oxide, 3. Define the micropatterns with lithography, 4. Etch oxide layer, 5. Etch surface microtopography with DRIE, 6. Clean the wafer, measure etched depths, dice the wafer into chips, soak in Piranha bath for 1-2 hours to clean and oxidize the surface. **B.** SEM images of the micropatterned surface. Insets show inner and outer ends on the 12 mm long microchannels.

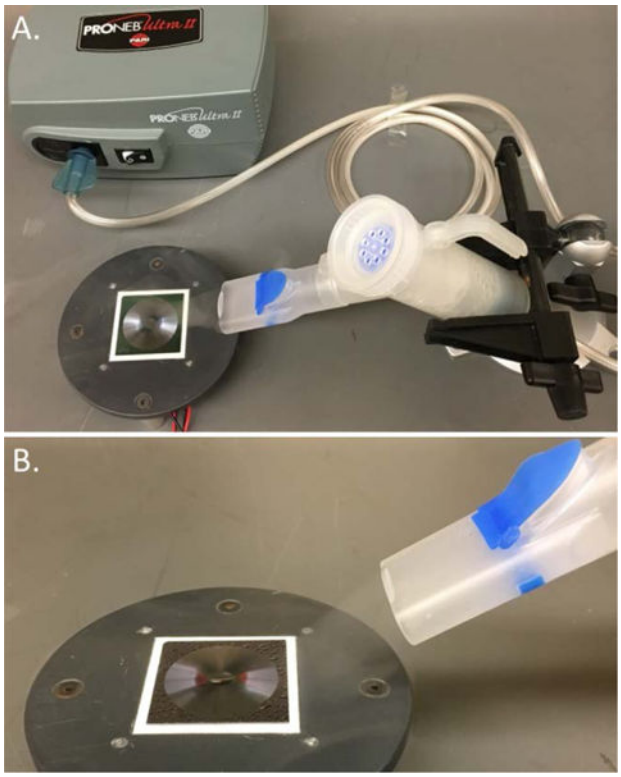

Figure 2.

A. Experimental set-up to observe the self-actuated condensate aggregation. **B.** Vapor flow over the surface is imitated with a nebulizer.

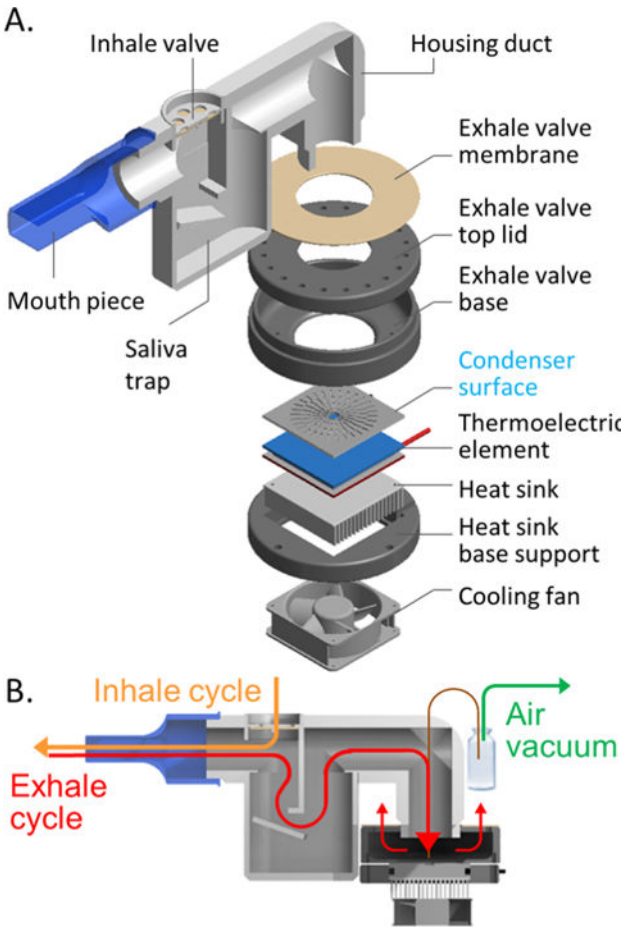

Figure 3.

Mini EBC sampler. **A**. Design and main components of the breath sampling device. **B.** Breath flow and sample extraction diagram.

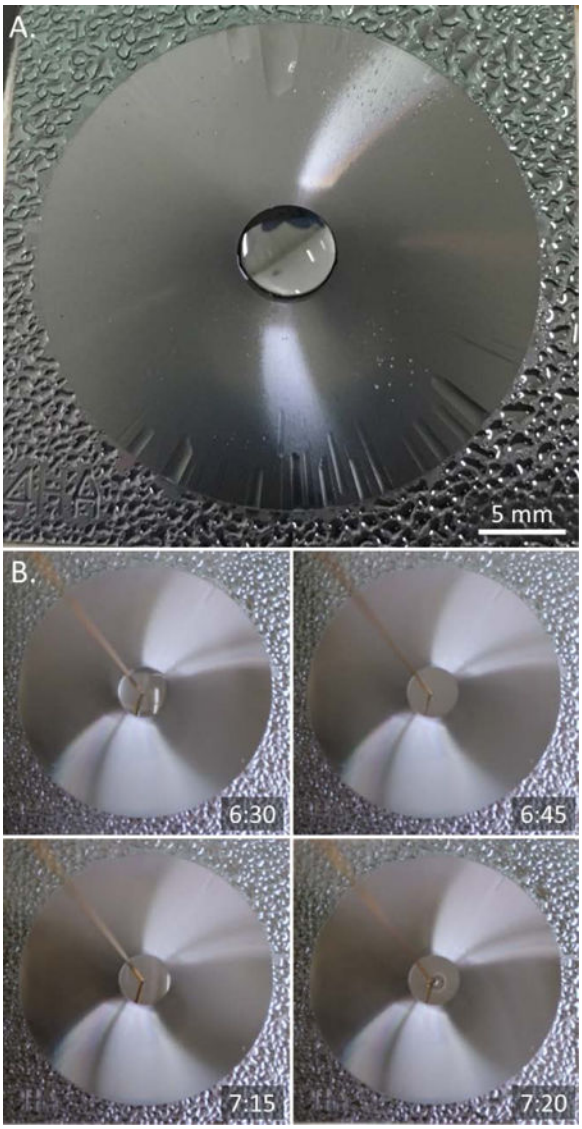

Figure 4.

Continuous condensation cycle. **A.** Capillary flow aggregates condensate liquid from the surface into a liquid dome. **B.** Rapid and repeatable self-aggregation of condensate liquid (6:30, 7:15) after extraction (6:45, 7:20) prevents surface saturation and allows collection of large sample volume on small surface area.

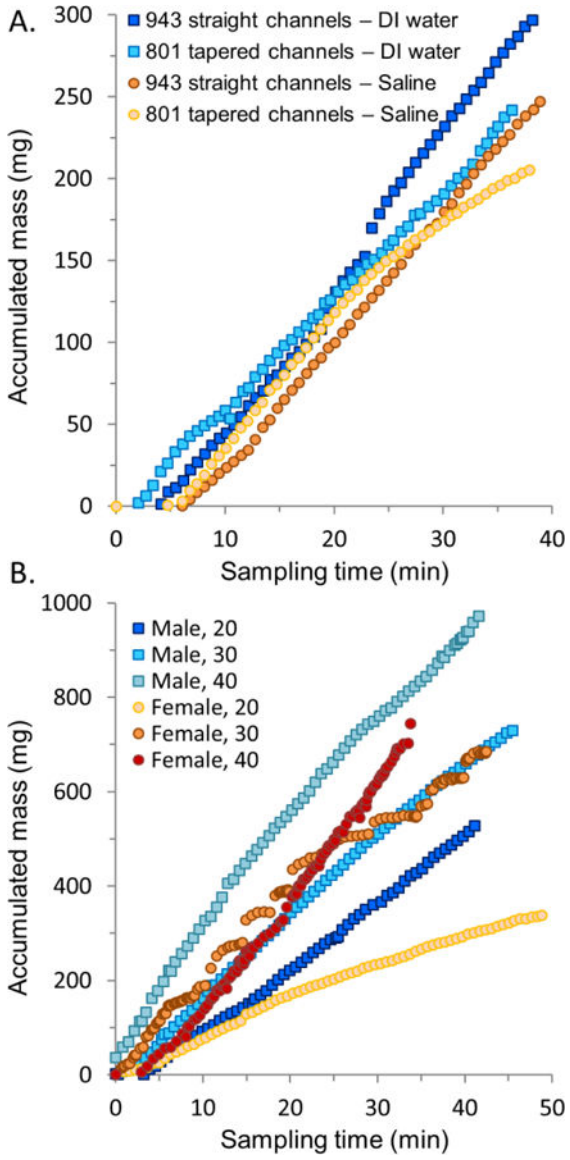

Figure 5.

Condensation rate in the mini EBC sampler. **A.** Sample accumulation rate with controlled flow. **B.** EBC sampling rate (mass/time) from six volunteers.

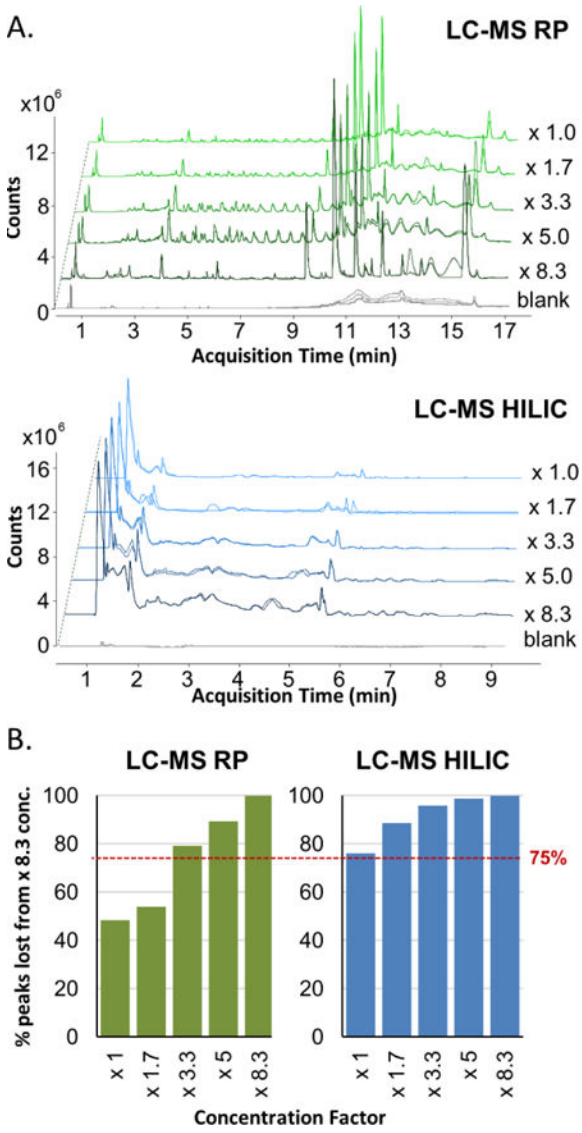

Figure 6.

Effect of sample volume on LC-MS analyses. **A.** Chromatographic profiles obtained at different concentration factors. The same scale of intensity (counts) was kept for all the chromatograms at different concentration factors. **B.** Percentage of lost peaks as a function of reconstituted sample concentration.

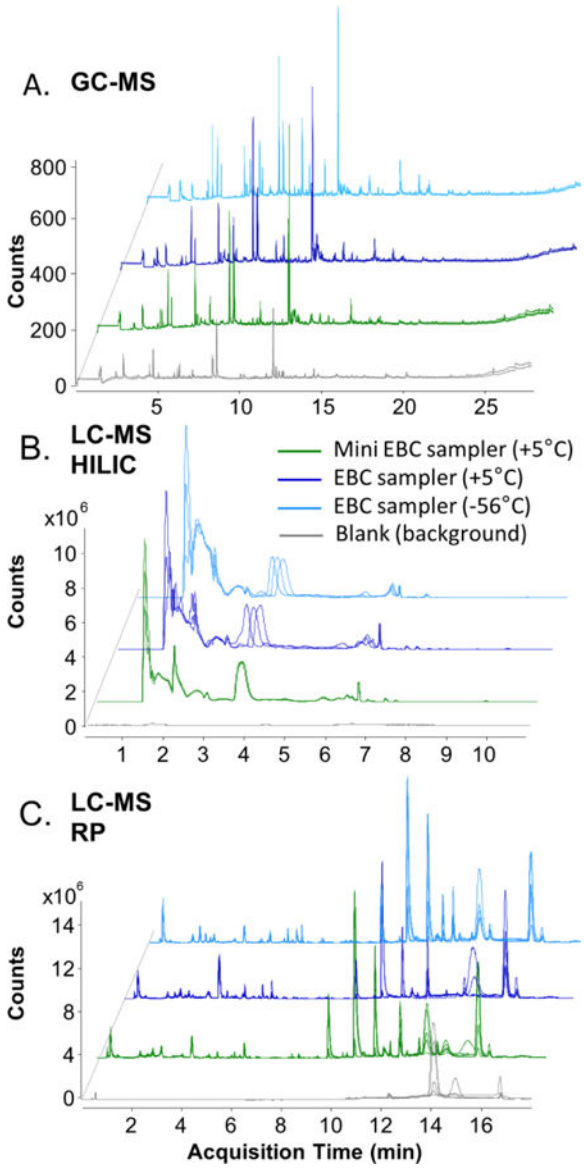

Figure 7.

Chromatographic profiles obtained with the two devices: mini EBC sampler (green) and glass tube EBC sampler (blues) considering the effect of temperature at +5 and −56°C. The same scale of intensity (counts) was kept for all the chromatograms at different concentration factors. **A.** GC-MS, **B.** LC-MS HILIC and **C.** LC-MS RP.

Table 1

Number of metabolites by device set-up and analytical method.

	LC-MS RP	LC-MS HILIC	GC-MS
mini-EBC sampler at +5°C	643	502	41
glass-EBC sampler at +5°C	675	600	41
glass-EBC sampler at −56°C	750	559	55